# Chapter 6

## Photoresponsive Magnetic Crossover

*In this chapter we present density functional theory based calculations on 6 diradicals in which imino nitroxide (IN) and IN or oxo- or phospha-verdazyl radical centers are linked by fragments of structures called cyan, blue and green fluorescent protein respectively. The photoinduced cis-trans isomerization of these diradical substituted chromophores is accompanied by changes from antiferro- to ferro-magnetic spin coupling on the radical centers. Moreover, upon irradiation with light of appropriate wavelength, the dark trans diradicals turn into their fluorescent cis isomers. Therefore, photoinduced magnetic crossover from antiferromagnetic to ferromagnetic regime associated with the change in color would be noticed in all three cases. This is a novel observation in case of the systems with green fluorescent protein chromophore and its variants. The change in color associated with magnetic crossover for these diradicals increases their suitability as biological taggers.*

## 6.1. Introduction

Photoresponsive green fluorescent protein (GFP) and its various mutants have been extensively used in biotechnology as well as in elemental and applied science research. GFP is stable and fluoresce at least up to 65°C temperature, which was first isolated in 1962 by Shimomura and co-workers from *Aequorea Victoria* jellyfish.[1] It is known to be responsible for the green bioluminescence of the jellyfish.[1,2] *Aequorea* GFP was the first such fluorescent protein for which the gene was cloned.[3] GFP is widely used to study the protein dynamics in living cells, in fluorescence microscopy, as a reporter gene, as a tagger in cellular biology and biotechnology, in transgenic plants, to study fungal biology, for protein localization in bacteria, to study embryos, as a vital marker in mammalian cell, in gene therapy, imaging biochemistry *in vivo*, visualizing chromosome dynamics, lighting up the cell surface, and so on, as have been nicely discussed in the comprehensive review of Zimmer.[4] Different transgenic living fluorescent species have also been developed using GFP.[5] Recently, it has been discovered that the GFP can act as light induced electron donors in photo biochemical reactions with various electron acceptors.[6] There are many other uses of GFP out side the laboratory.[7] Moreover, National Aeronautics and Space Administration (NASA) have developed a GFP Imaging System (GIS), a controlled nondestructive analytical tool to judge the status of a target organism in stellar objects. This device is likely to revolutionize space biological research by eventually eliminating the resource intensive requirement to return biological materials to earth for post flight analysis. This advanced technique can be applied to a host of model organisms engineered with the GFP gene construct including plants, microbes, and nematodes.[8]

The chromophore of GFP is a *p*-hydroxybenzylidene imidazolinone derivative (*p*-HBI) formed by self-catalyzed covalent modification of Ser65-Tyr66-Gly67 residues.[4] Spontaneous rearrangement and oxidation of Ser-Tyr-Gly residue is the source of fluorescence in GFP. The crystal structure study of GFP shows that it contains a unique 11-strand β-barrel fold structure with a central helix containing the fluorophore which plays a significant role in its fluorescence properties. With relatively small molecular mass (27 kDa), the thermostable GFP composed with 238 amino acids can tolerate both N- and C-terminal

protein fusion.[2] When the fluorophore is irradiated with ultra violet (UV) or blue light it emits green light.[2,4] Aequorin, which is a luciferase, contains coelenterazine the luciferin, and GFP are the two proteins which are involved in bioluminescence in wild *Aequorea* jellyfish. Aequorin binds with three calcium ions to oxidize coelenterazine to form $Ca_3$-apo-aequorin-coelenteramide complex which *in vitro* emits blue light. Instead of giving blue bioluminescence the aequorin complex *in vivo* undergoes radiationless energy transfer to GFP which then gives off green fluorescence.[4] Once excited by light of 488-nm wavelength, it undergoes repeated cycle of fluorescent emission i.e., "blinking" for several seconds. This behavior indicates that it can act as an optical storage material, molecular photonic switch or fluorescent marker.[9] To change the photophysical features, several mutants of GFP have been designed by genetic engineering and some of them are already synthesized and characterized. Three different isomers of dimethyl derivative of GFP chromophore *o*-HBDI, *p*-HBDI and *m*-HBDI have been synthesized and characterized.[10,11] Chromophores of GFP (Ser65-Tyr66-Gly67) analogue are obtained from similar chemical modification with the only difference is that they are formed with other tripeptide chains. Replacing Tyr66 with Trp-, His-, Phe-residues (i.e., triptophan, histidine or phenylalanine) one can get different blue shifted variants of GFP such as, cyan fluorescent protein (analogue of Y66W GFP i.e., CFP), blue fluorescent protein (analogue of Y66H of GFP i.e., BFP), and BFPF (analogue of Y66F GFP) respectively. Thus, when indolyl or imidazolyl or phenyl ring replaces the phenol of GFP moiety, a blue shifted fluorescence is observed; in spite of low quantum yield these mutants perform multidimensional biological applications. All these above mentioned synthetic chromophores undergo photochromic cis/trans isomerization upon irradiation. However, it is to be noted here that Matsuda and co-workers[12] have also isolated and characterized various photochromic spin couplers. Theoretically, Ali and Datta have investigated the photomagnetic behaviour of nitronyl nitroxide, imino nitroxide and verdazyl derivatives of substituted pyrene and found that magnetic coupling constants changed their magnitude when exposed to electromagnetic radiation of right frequency.[13] In a recent work, it has been shown that photochromic antiferromagnetic to ferromagnetic crossover occurs in organic magnetic entity when exposed to light of suitable wavelength.[14] This leads us to focus on the design and investigation of magnetic systems with synthetic analogue of GFP and its different photochromic variants, where photoresponsive antiferromagnetic to ferromagnetic crossover occurs. These prospective biocompatible diradicals undergo magnetic crossover

along with change in color, as a result they are likely to be more useful in different *in vivo* treatments as already discussed. As substituted dark nonfluorescing trans GFP chromophore converts into its bright fluorescing cis isomer when exposed to light,[15] GFP coupler can be suitably crafted between two radical centers so as to produce a photochromic and photoactive reversible diradical which can undergo magnetic crossover with irradiation of light of appropriate wavelength.

**Scheme 6.1.** Photoinduced conversion of diradicals from trans isomer to cis isomer, where GFP chromophore and its variants are used as couplers. Here, $\tau$ and $\varphi$ are the two stereochemically relevant dihedral angles.

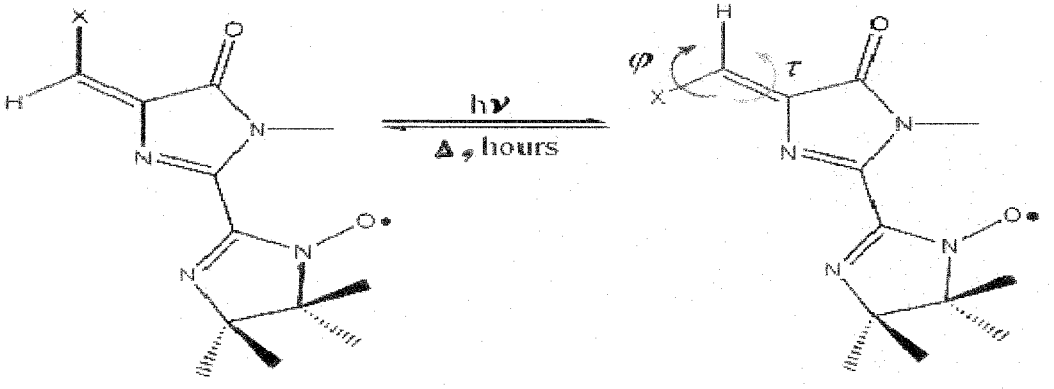


Trans (*E*) (a) Cis (*Z*) (b)

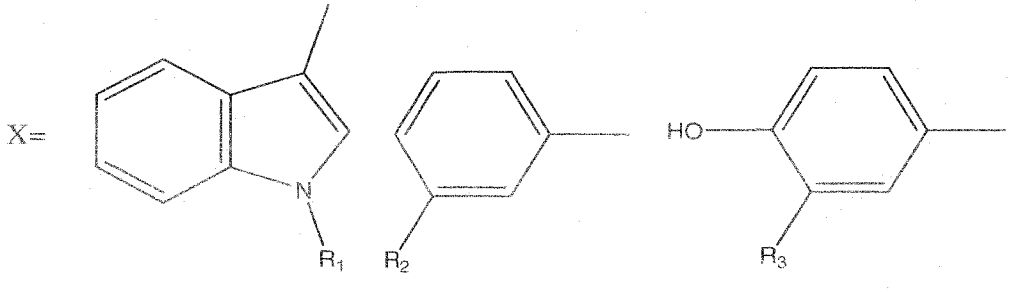


1 2 3

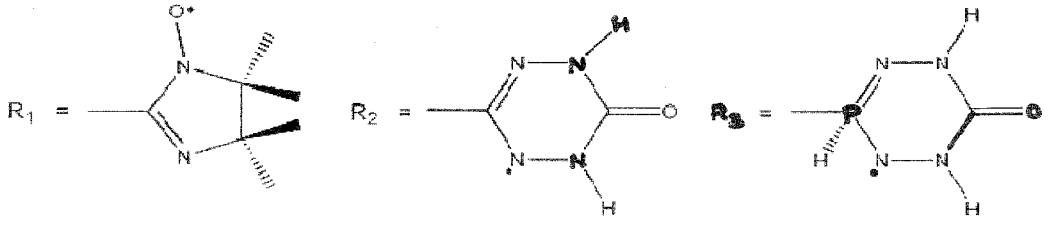


Iminonitroxide Oxoverdazyl Phosphaverdazyl

In GFP like chromophores, generally the cis isomer possesses lower energy than the corresponding trans form.[16] The cis and trans isomers of synthetic analogues of GFP and BFPF are characterized by the rotation of symmetrical phenol and phenyl rings around φ, but in case of CFP, the presence of asymmetric indolyl ring disrupts this symmetry of rotation (Scheme 6.1). Both the cis CFP and trans CFP chromophores are characterized by two energy minima.[15] Here, in this study we take more stable trans CFP configuration as well as its cis form. Radicals of imino nitroxide (IN) family are known to be stable and they are also used to design molecular magnets.[17] Nearly planar or planar verdazyl molecules are attractive alternative to nitroxides as through space interactive building blocks.[18] In this chapter, we design six diradicals with GFP chromophore and its variants (i) CFP as a coupler with two IN moieties act as radical centres in diradicals 1a and 1b; (ii) BFPF as a coupler with oxoverdazyl and IN moieties are the two different radical centres as in diradicals 2a and 2b; and (iii) dimethyl substituted synthetic GFP chromophore (*p*-HBDI) as a coupler with phosphaverdazyl and IN moieties are two different radical centres as in diradicals 3a and 3b (Scheme 6.1), and predict the photoinduced magnetic behaviour therein. Among these molecules 1a, 2a and 3a are the trans isomers, whereas 1b, 2b and 3b are their corresponding cis forms respectively.

## 6.2. Theoretical Background and Methodology

The interaction between two magnetic sites 1 and 2, is generally expressed by the Heisenberg spin Hamiltonian

$$\hat{H} = -2J\hat{S}_1 \cdot \hat{S}_2, \tag{6.1}$$

where $\hat{S}_1$ and $\hat{S}_2$ are the respective spin angular momentum operators and $J$ is the exchange coupling constant. The positive sign of $J$ signifies the ferromagnetic interaction while the negative value indicates the antiferromagnetic interaction. For a diradical containing one unpaired electron on each site, $J$ can be represented as

$$E_{(S=1)} - E_{(S=0)} = -2J\,. \tag{6.2}$$

Due to spin contamination, the single determinantal wave function cannot satisfactorily represent a singlet state of a diradical in the unrestricted formalism. To overcome this problem one may prefer multiconfigurational approaches to obtain pure spin states. However, these methods are resource intensive and not being used in this chapter. Broken symmetry (BS) approach given by Noodleman[19] in DFT framework is an alternative route to evaluate *J*, which is more effective due to less computational effort. BS state is an artificial state of mixed spin symmetry and lower space symmetry. The BS solution is often found to be spin contaminated, and using spin projection technique one can overcome this problem. Depending on the extent of magnetic interaction between two magnetic sites, many researchers have developed diverse formalisms to assess *J* using unrestricted spin polarized BS solution.[19-25] The equation for evaluating *J* proposed by Ginsberg,[20] Noodleman[21] and Davidson[22] is applicable when interaction between two magnetic sites is small. On the other hand, the expression given by Bencini [23] and co workers and Ruiz et al., [24] is applicable for large interaction. Nevertheless, the eminent expression given by Yamaguchi[25] is relevant for both strong and weak overlap limits. Following the well established and widely applied method,[13,26] we use the Yamaguchi[25] formula for evaluation of *J* value in this chapter, which is given by

$$J = \frac{(E_{BS} - E_{HS})}{\langle S^2 \rangle_{HS} - \langle S^2 \rangle_{BS}}, \tag{6.3}$$

where, $E_{BS}$, $E_{HS}$ and $\langle S^2 \rangle_{BS}$, $\langle S^2 \rangle_{HS}$ are the energy and average spin square values for corresponding BS and high spin states.

It is necessary to say that, in this chapter, we have used a simple and widely employed approximation to estimate the spin state preference. An estimate of the open shell singlet energy is obtained by broken symmetry wave functions using unrestricted formalism. It is widely accepted that this produces an equal mixture of singlet and triplet states. However, Neese[27] has advocated over the fact that these states are not equally mixed as it thought to be. Moreover, projection of the triplet leaves a singlet component. For diradicals, $\langle S^2 \rangle$ = 1

represents pure BS state. The singlet states are spin contaminated in DFT formalism, and the MOs are not optimized for an open shell singlet. The MOs are optimized for the triplet and these are used to estimate the BS state, as a result, this calculation tends to be biased in favor of the triplet. Here, we estimate the singlet and triplet weightage in the computed BS solutions for each diradical. Another point needs to be noted here that, in molecular level a quantitative calculation of first and second energy derivatives, which are influenced by spin contamination is of significant interest. Recently Yamaguchi and co-workers[28] have used a new method to avoid such spin contamination from geometry optimization using approximate spin projection (AP) procedure, but this procedure is resource intensive and not being employed in the chapter.

Generally, in any photoinduced process it is necessary to know the excitation energy. In GFP chromophores and its variants, the excitation would take place from bonding to antibonding $\pi$ orbitals. Here, we calculate electronic excitation energies with time-dependent density functional theory (TDDFT) which is essentially a DFT analogue of time dependent Hartee–Fock (TDHF) approach using B3LYP functional with 6-31G(d,p) basis set. In TDDFT the fundamental variable is time dependent density and exchange correlation potential describes many body interactions.[29] TDDFT in early days is considered only for the closed shell molecules by describing singlet–singlet or singlet–triplet excitation dominated by single electron excitation. Recently it has been shown that TDDFT is also useful to estimate excitation energies of open shell molecules.[30] However, in any photoinduced process, $\pi \rightarrow \pi^*$ transition energy can be calculated through time dependent perturbative technique. It is known that there arise inherent errors due to "near triplet instability" in prediction of transition energy through time dependent Hartree–Fock method (TDHF).[31] Hartee–Fock (HF) based single excitation theories, configuration interaction singles (CIS) method, have many similarities with TDHF method. CIS avoids the problem of "near triplet instability" error as it is not a response theory method, even though its results are not precise enough as evident in numerous applications. Many post Hartree Fock *ab initio* methods are free from such errors; however, being computationally expensive not been employed in this chapter. On the other hand, TDDFT is more robust than TDHF and CIS, and known to produce minimal "near triplet instability" error,[32] hence, the TDDFT method is used in this

chapter to calculate excitation energies. The TDDFT method is based on the dynamic polarizability $\bar{\alpha}(\omega)$ of a system which has poles at frequencies analogous to its transition energies. Obtaining the frequency dependent polarizability from TDDFT calculations and substituting it in the relation

$$\bar{\alpha}(\omega) = \sum_I \frac{f_I}{\omega_I^2 - \omega^2}, \tag{6.4}$$

one can get oscillator strength ($f_I$) and excitation frequency ($\omega_I$) respectively.[31] In this chapter, we calculate $\pi \rightarrow \pi^*$ transition energies for all substituted trans fluorescent protein chromophores following the method mentioned above.

## 6.3. Results and Discussion

In this chapter, the molecular geometries of all six molecules have been fully optimized by hybrid exchange-correlation functional B3LYP using 6-31G(d,p) basis set within the unrestricted formalism. The optimized geometries are shown in Figure 6.1. Based on these molecular geometries the corresponding $J$ values for each molecule have been estimated from the energies of the triplet and BS states at same level of theory. To obtain open shell BS singlet solution "guess =mix" keyword is used within unrestricted formalism. The BS states for all six diradicals are stable. To confirm the stability of BS solution, we follow the procedure developed by Bauernschmitt and Ahlrichs,[33] which is an extension of the SCF stability analysis given by Čížek and Paldus.[34] This has been implemented in this chapter by using "stable" keyword. All the calculations have been carried out using GAUSSIAN 03W[35] quantum chemical package.

The cis isomers of these chromophores are known to possess lower energy than corresponding trans isomers or zwitterionic species either in gas phase or in solution.[4,15] In the optimized structures (Figure 6.1) of the trans diradicals (1a, 2a, 3a), the atoms containing the unpaired spins and the couplers are in the same plane. The trans diradicals have singlet ground state, so the polarization of spin in the high spin state of these molecules through the

fluoro protein couplers is blocked and hence antiferromagnetic behaviour is observed in such cases (Figure 6.2), this is also in good agreement with spin alternation rule.[36] On the other hand, in cis diradicals (1b, 2b, 3b), the radical centres are slightly out of plane with a very low dihedral angle ($\varphi$ = 1.07°, −2.76° and −2.71° and $\tau$ = 0.27°, −0.74°, −0.63° for diradicals

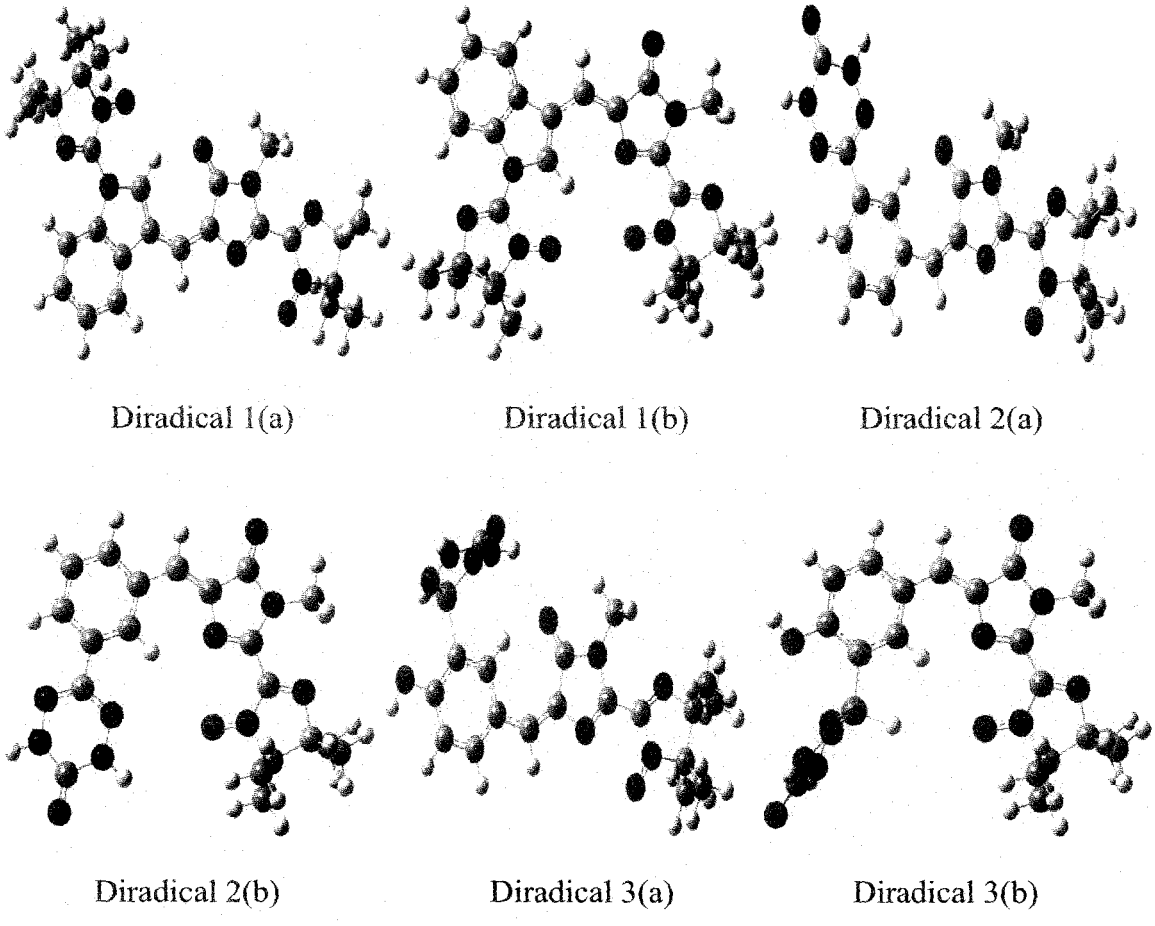


**Figure 6.1.** The optimized geometries of three trans (1a, 2a, 3a) diradicals and their corresponding cis forms (1b, 2b, 3b) with different GFP variants (CFP, BFPF and *p*-HBDI respectively) as coupler from UB3LYP/6-31G(d,p) calculations. The carbon atoms are represented in grey, nitrogen in blue, oxygen in red, phosphorus in orange, and hydrogen in white respectively.

1b, 2b, 3b correspondingly). The dihedral angles $\varphi$ and $\tau$ are shown in Scheme 6.1. Moreover, in the cis forms radical centres are also closer in space compared to that in the trans diradicals. Proximity of the radical centres in cis isomers facilitates direct exchange,

which usually favours the ferromagnetic coupling.[14] As a result, cis diradicals show ferromagnetic behaviour with the triplet ground state. The spin alternation rule is less pronounced in these cases where the radical sites are close to each other,[14] which is also obvious from spin density plots (Figure 6.2).

We have calculated the value of $J$ for all three systems in the cis and trans forms. The energy and $\langle S^2 \rangle$ values for both triplet and BS states are reported in Table 6.1. Here, the $J$ values of all three species in the trans forms are negative, but in the case of cis forms, $J$ values are positive. Thereby from the point of view of basic principles of magnetism one may note that all trans forms have spins with opposite orientations in two spin sites and similarly all cis forms have spins with same alignments in two radical centers, i.e., antiferromagnetic and ferromagnetic situations in respective cases being observed. This is also obvious from

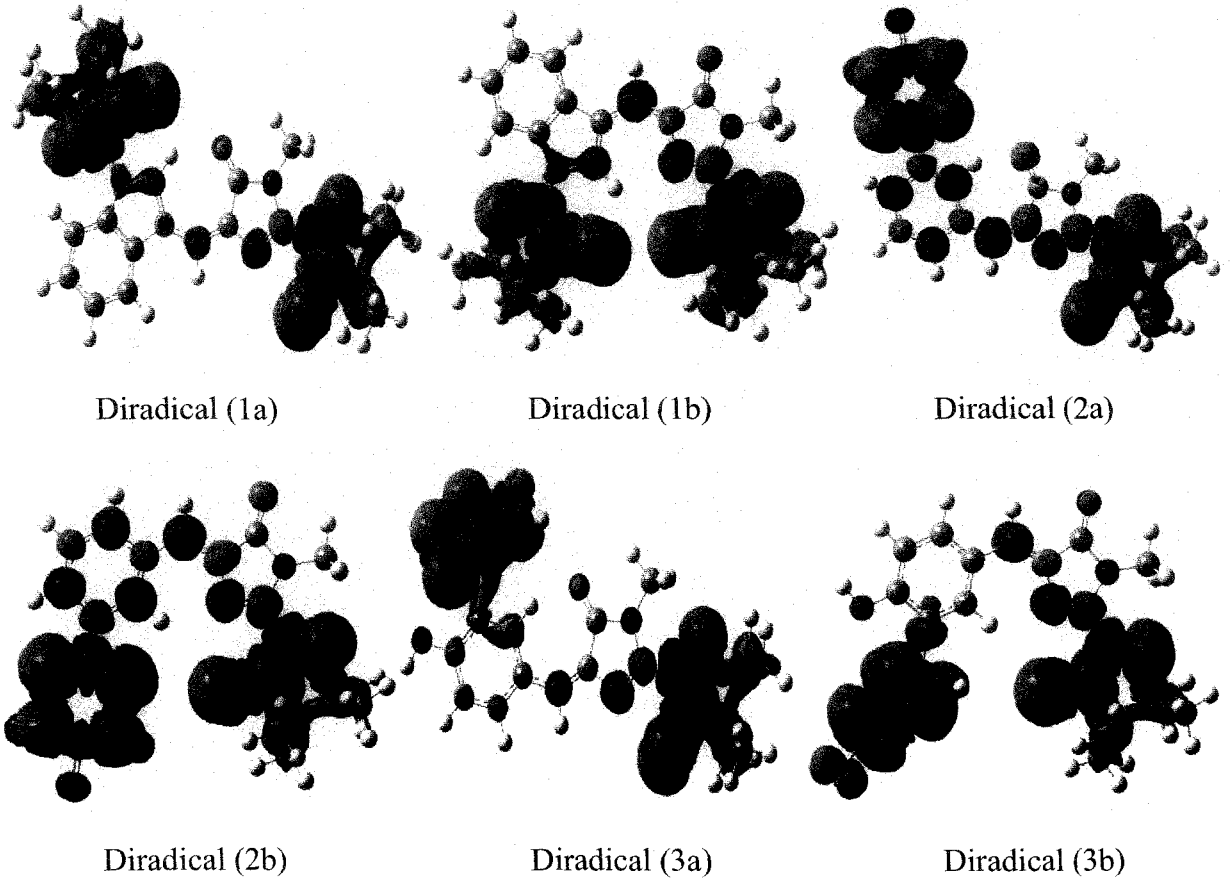


**Figure 6.2.** Spin density plots for the diradicals in their triplet states; green color indicates up spin and red color indicates down spin.

spin density maps in Figure 6.2. As a result, a magnetic crossover from antiferro to ferro would be noted in all three cases when the trans isomers are subjected to photoisomerization. It is also to be noted that, potential energy of a diradical system has two wells corresponding to the two stable orientations of the magnetism. In case of conventional magnetic reversal by applying magnetic field one of the two wells become metastable when small field is applied. At a particular field, whose frequency matches the precision frequency of the magnetization called the switching field, the energy can be pumped into the system and the energy barrier between the two wells vanishes, as a result magnetization reverses. This magnetic field induced magnetization reversal in magnetically active materials is a fundamental issue in many applications and it is difficult to implement as it requires very high field gradient.[37] On the other hand, photoinduced magnetic crossover is easy to implement and expected to find wide applications. The cis and trans forms of GFP chromophore and its variants have different absorption spectra and these two forms can be converted to each other i.e., their structures and physical properties can change when exposed to proper electromagnetic radiation. Since the trans form of all the diradicals are dark, upon irradiation of light of suitable wavelength on the dark trans isomers corresponding bright fluorescing cis forms (cyan, blue and green colors for diradicals 1b, 2b and 3b respectively) are obtained.[2,15] As a result, here we observe different states of magnetism with different colors, that is, it is easy to understand the magnetic property of these six diradicals by visual inspection even without evaluating coupling constants.

The photoisomerization from diradical (a) to diradical (b) [in every case (1-3)] is initiated by $\pi \rightarrow \pi^*$ transition energy, hence, we calculate the transition energies for trans isomers of each diradical. The experimentally observed excitation peaks for neutral bare couplers in 1a, 2a and 3a diradicals are 436 nm, 360 nm, and 399 nm respectively.[2] Transition energies obtained by TDDFT method are known to be less dependable due to spin contamination.[38] However, many authors have found good agreement between calculated transition energies and experimental values using TDDFT methods.[39,40] Thus, it has been prudently surmised that TDDFT calculations for open shell molecules are very reliable to explain experimental results even it lacks a solid theoretical background.[39] In our TDDFT calculations for diradicals 1-3 (Table 6.2), we get reasonable agreement with previous

experimental results for the respective chromophores.[2] Hence, upon irradiation with light of 360-390 nm wavelengths the trans isomers would be converted into their corresponding cis forms, as a consequence structural isomerization with magnetization reversal from antiferro to ferro associated with change in colors would be observed. It is apparent from other works[2,4] that electronic transition in the GFP like chromophores leads to fluorescence decay. Therefore, it may be argued that in the present case even if a part of the excited molecules fluoresce through $S_1 \rightarrow S_0$ transition, a sizable amount may undergo intersystem crossing (ISC) to the triplet $T_1$ state which eventually decays energy via nonradiative pathways. A general schematic representation of the photoresponse for all of our designed diradicals is given in Scheme 6.2.

**Table 6.1.** UB3LYP level absolute energies in *au*, $\langle S^2 \rangle$, and exchange coupling constants ($J$ in $cm^{-1}$), using 6-31G(d,p) basis set for trans and cis forms of all diradicals.

| Diradicals | | At UB3LYP/6-31G(d,p) level | | |
|---|---|---|---|---|
| | | Energy(*au*) | $\langle S^2 \rangle$ | $J(cm^{-1})$ |
| 1a | Triplet | –1657.61021 | 2.032 | –20 |
| | BS | –1657.61030 | 1.034 | |
| 1b | Triplet | –1657.61180 | 2.032 | 9 |
| | BS | –1657.61176 | 1.032 | |
| 2a | Triplet | –1438.97996 | 2.050 | –2 |
| | BS | –1438.97997 | 1.046 | |
| 2b | Triplet | –1438.98505 | 2.052 | 35 |
| | BS | –1438.98489 | 1.046 | |
| 3a | Triplet | –1817.99078 | 2.025 | –15 |
| | BS | –1817.99085 | 1.025 | |
| 3b | Triplet | –1817.99461 | 2.027 | 13 |
| | BS | –1817.99455 | 1.028 | |

**Table 6.2.** The $\pi \rightarrow \pi^*$ transition energy values, estimated wave length $^{a}\lambda_{exc}$ in trans diradicals at UB3LYP (TDDFT) level using 6-31G(d,p) basis set, $^{b}\lambda_{exc}$ is the experimental value for bare coupler from ref. 15(a).

| Diradicals | $E_{\pi}$ in *au* | $E_{\pi^*}$ in *au* | Transition energy in *eV* | Estimated $^{a}\lambda_{exc}$ for diradicals in nm | Experimental $^{b}\lambda_{exc}$ for bare couplers in nm |
|---|---|---|---|---|---|
| 1a | –0.19374 | –0.07620 | 3.1985 | 387 | 436 |
| 2a | –0.21580 | –0.09002 | 3.4227 | 361 | 360 |
| 3a | –0.21349 | –0.08939 | 3.3770 | 366 | 399 |

**Scheme 6.2.** A general schematic representation of the photoresponse for all of our designed diradicals, where $S_0$, $S_1$, and $T_1$ are the singlet electronic ground state, singlet electronic excited state and triplet electronic excited state respectively. ISC represents intersystem crossing.

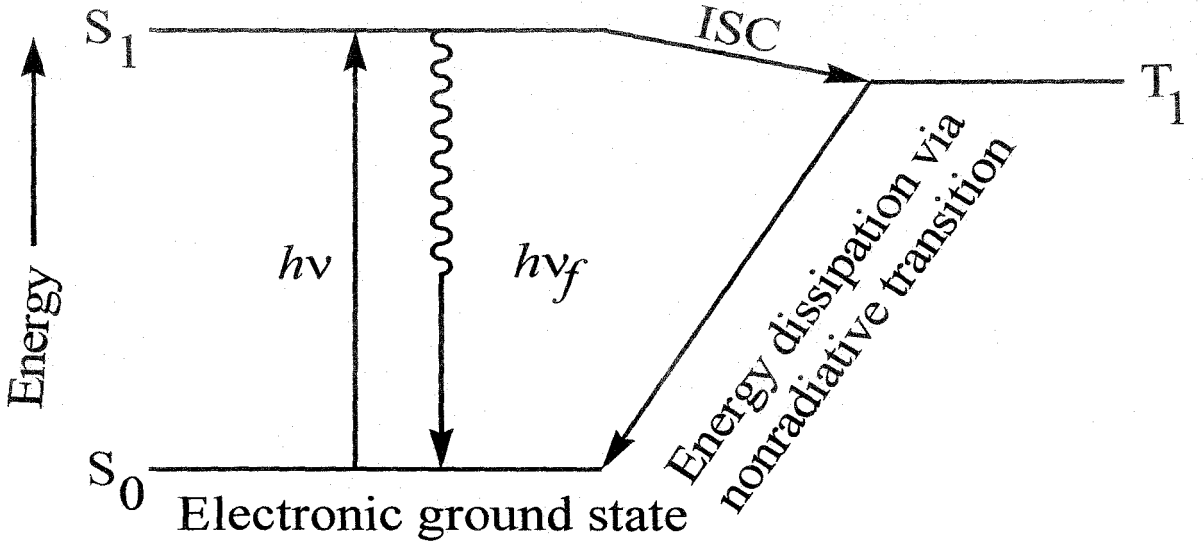


The up-spin density on both radical sites is intense as obvious from spin density plots (Figure 6.2), hence spin-up electrons will go through the molecules from one magnetic sites to another when bias is applied, whereas the propagation of spin-down electrons are

blocked.[41] Using GaussSum v. 2.1 software,[42] the density of states (DOS) plots (Figure 6.3) are evaluated from the output file of population analysis obtained using Gaussian 03W.[35] From DOS plots one can find very easily that the spins are highly polarized at Fermi level in bright ferromagnetic cis diradicals, whereas in case of dark trans diradicals no such polarization is observed. Thus ferromagnetic cis diradicals can show spin valve effect, that is, the majority spins are conveyed only in one direction when bias is applied.[41] It is also noted that in case of diradicals 1b and 3b, the $\beta$-HOMO is located above the Fermi level. This observation is due to non-Aufbau occupation of molecular orbitals (MOs) in these cases. Non-Aufbau behavior is experimentally and theoretically supported by Westcott et al.[43] Aufbau principle can also be violated due to delicate balance between promotion energies, coulomb repulsions and exchange interactions.

Diradical 1(a)

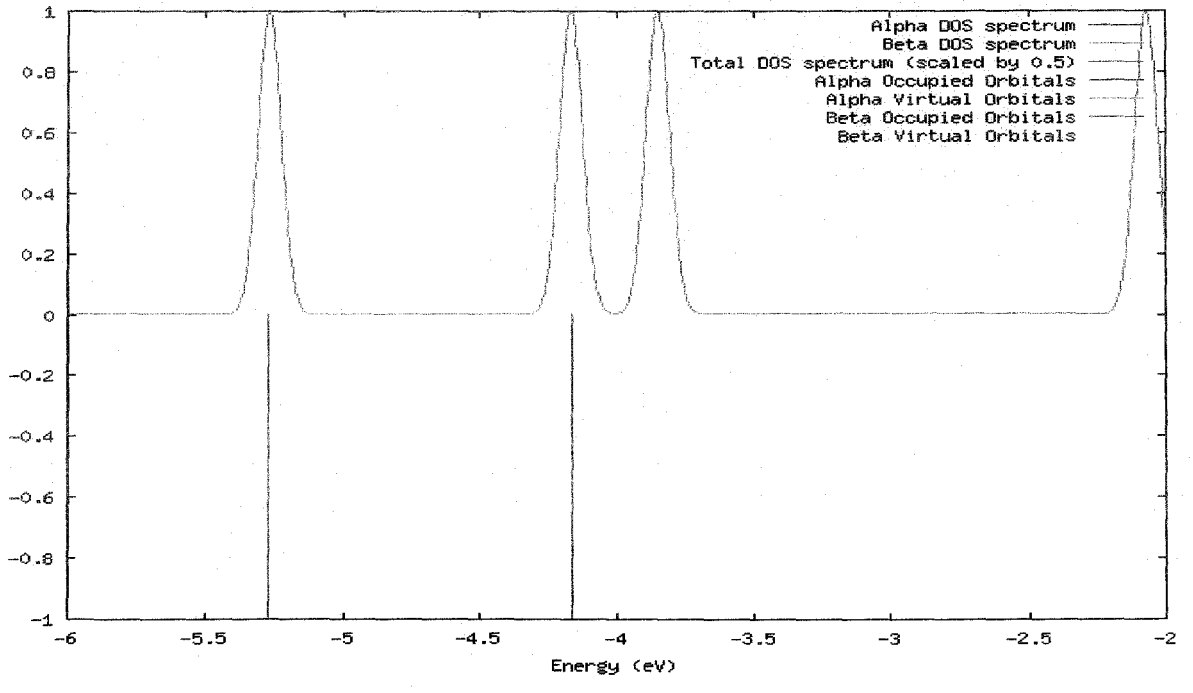

Diradical 1(b)

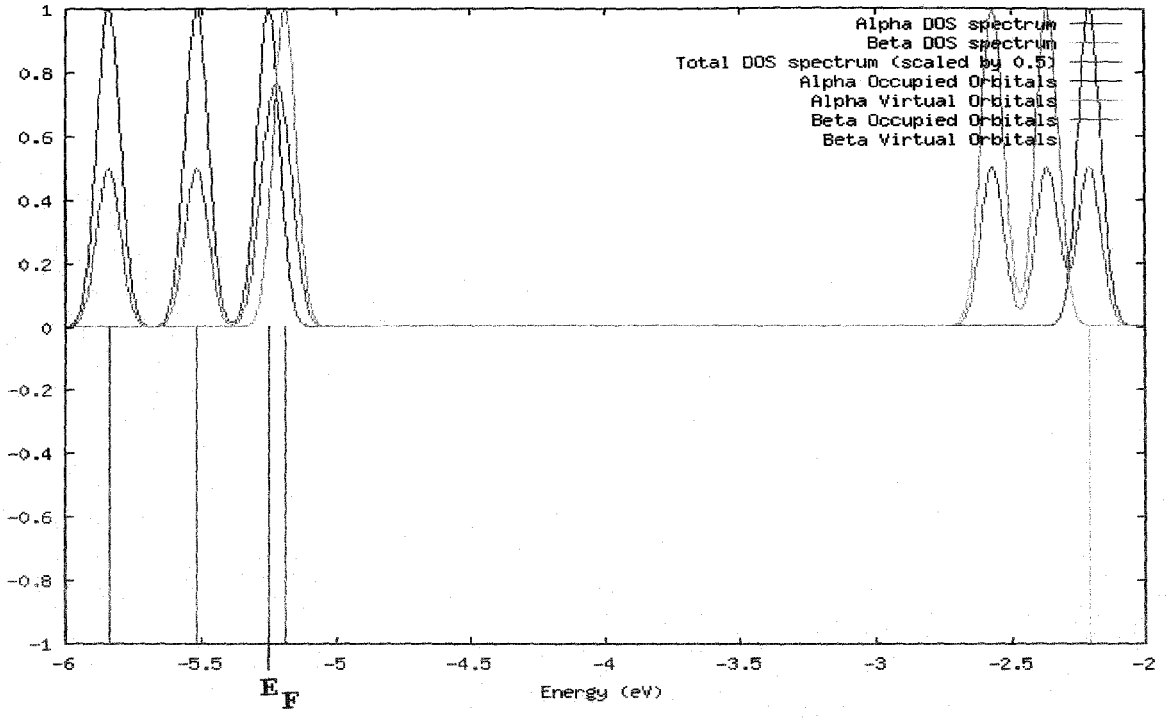


Diradical 2(a)

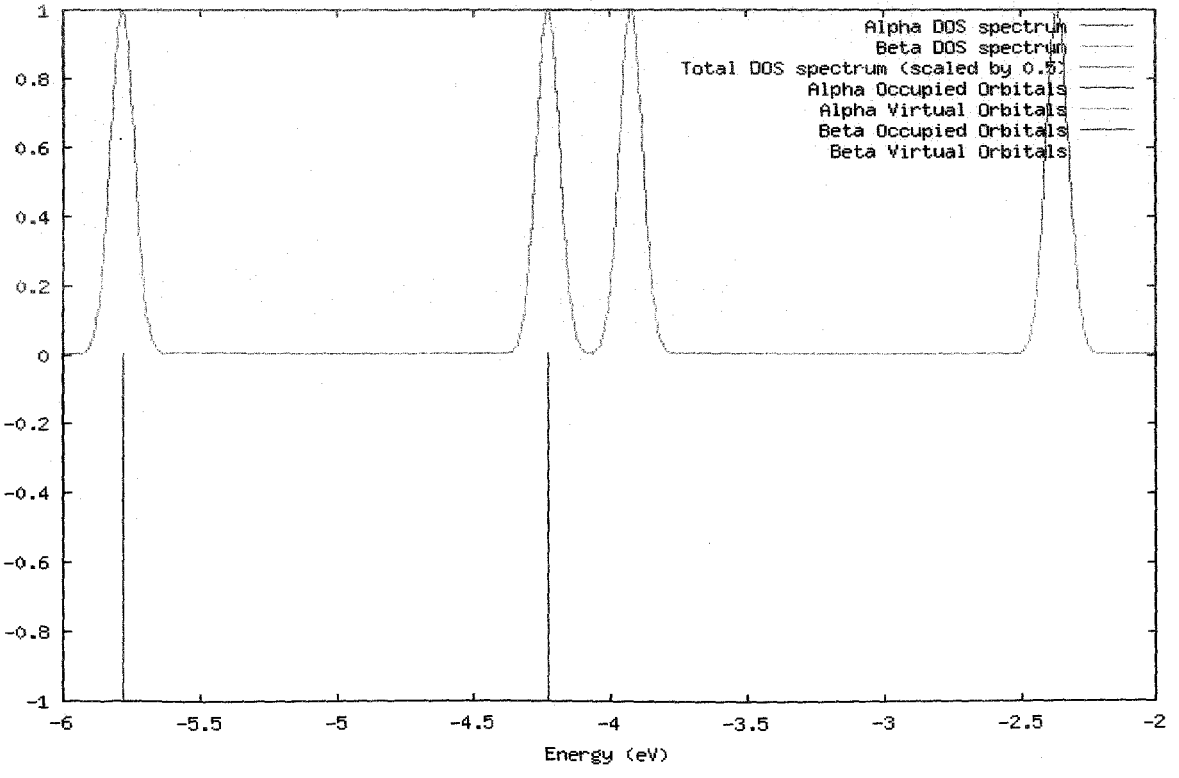

Diradical 2(b)

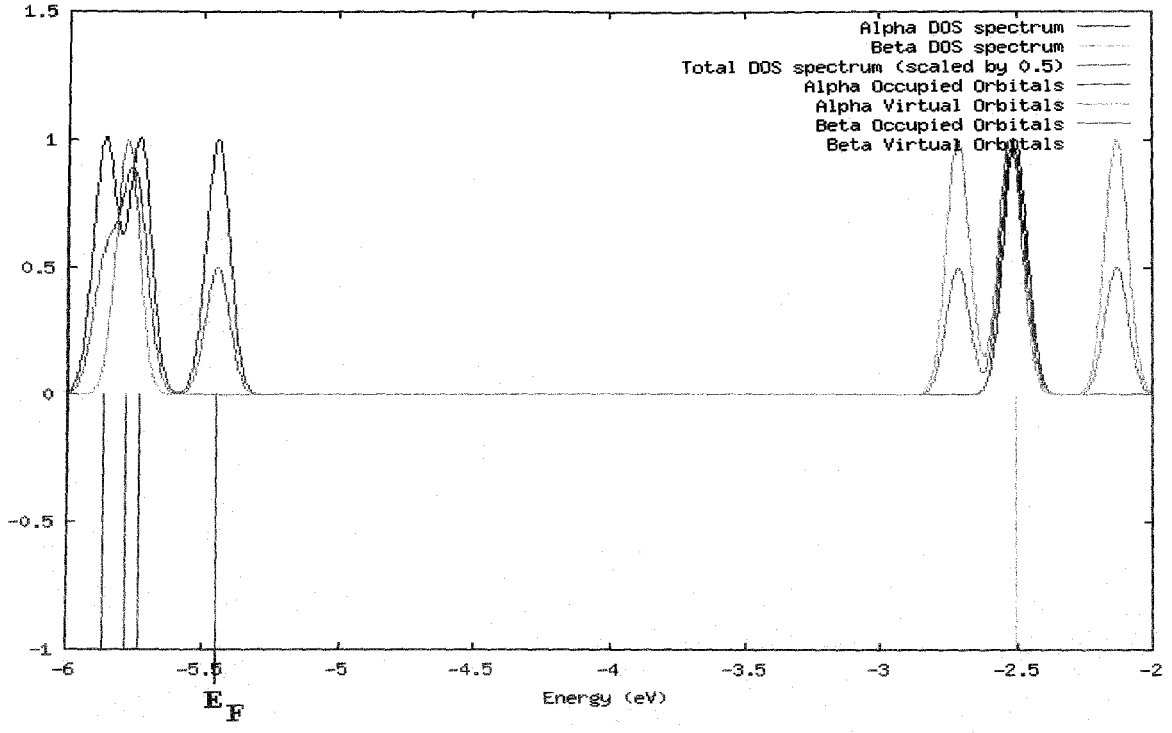


Diradical 3(a)

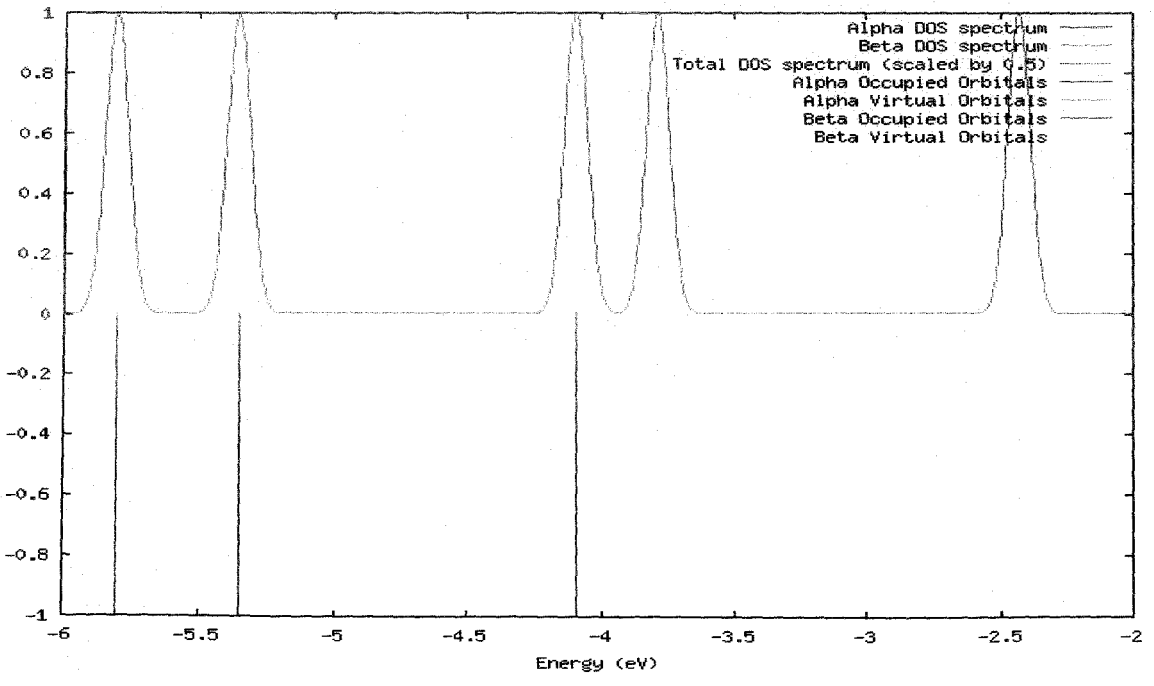

Diradical 3(b)

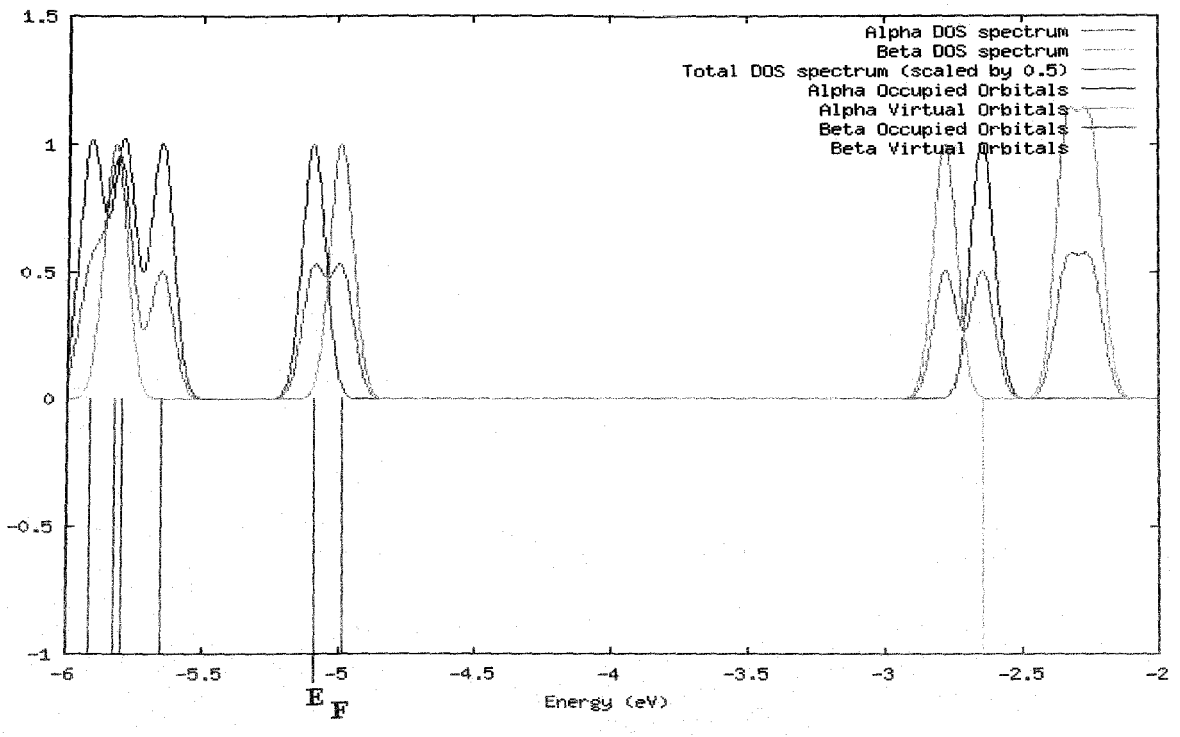


**Figure 6.3.** DOS vs energy plots for antiferromagnetic trans (1a, 2a and 3a) and their respective ferromagnetic cis (1b, 2b and 3b) isomers, consequent Fermi levels are indicated as $E_F$.

A discussion on estimated singlet and triplet weightage for each diradicals is due here. These estimated values are given in Table 6.3. For this calculations, in pure state, we take the broken symmetry wave function, $\psi_{BS} = m\ \psi_S^{BS} + n\ \psi_T^{BS}$, where $\psi_S^{BS}$ and $\psi_T^{BS}$ singlet and triplet component functions, and $m^2 \approx n^2 = \frac{1}{2}$, that is, $m^2 + n^2 = 1$. Also $n^2 = \frac{1}{2}\langle S^2 \rangle_{BS}$, so that, $m^2 = 1 - \frac{1}{2}\langle S^2 \rangle_{BS}$. It is obvious from Table 6.3 that for both ferromagnetic and antiferromagnetic species the triplet weightage is greater in every case as also obvious from the work of Datta and co-workers.[45]

**Table 6.3.** Percent net weight of singlet and triplet components in the computed BS Solution, using $50\langle S^2\rangle_{BS}$ and Singlet weightage = 100 – Triplet weightage.

| Diradicals | Singlet % Weightage ($100m^2$) | Triplet % Weightage ($100n^2$) |
|---|---|---|
| 1a | 48.30 | 51.70 |
| 1b | 48.40 | 51.60 |
| 2a | 47.70 | 52.30 |
| 2b | 47.70 | 52.30 |
| 3a | 48.75 | 51.25 |
| 3b | 48.60 | 51.40 |

We have compared the ground state stability of the cis and trans forms of these fluoro proteins coupled diradicals. Commonly, ferromagnetic diradicals show greater stability than their antiferromagnetic counterparts,[45] as also apparent from Table 6.4. Nonetheless, the estimated singlet state energy ($E_S$) values for trans diradicals are lower than the respective computed triplet state energy values ($E_T$ ) ( Table 6.1 and Table 6.4), i.e., singlet ground states for trans diradicals are confirmed.

**Table 6.4.** Ground state energies of six diradicals from single point UB3LYP/6-31G(d,p) calculations.

| Diradicals | Estimated $E_s$ in *au* | Diradicals | $E_T$ in *au* |
|---|---|---|---|
| 1a | –1657.61039 | 1b | –1657.61180 |
| 2a | –1438.97998 | 2b | –1438.98505 |
| 3a | –1817.99092 | 3b | –1817.99461 |

The energy differences between the $\alpha$–highest occupied molecular orbital ($\alpha$–HOMO) and $\alpha$–lowest unoccupied molecular orbital ($\alpha$–LUMO) for all 6 molecules (Table 6.5) have been evaluated. The energy gap also corresponds to the chemical hardness of the molecule. Chemical hardness is calculated from the formula, $\eta = (E_{LUMO}-E_{HOMO})/2$, where $\eta$ is the molecular hardness, $E_{LUMO}$ and $E_{HOMO}$ are the energy of the LUMO and HOMO respectively. From Table 6.5, it is evident that all the cis diradicals have lower HOMO–LUMO energy gap than the corresponding antiferromagnetic trans isomer, which implies that lower molecular hardness and the higher molecular polarizability is observed for ferromagnetic cis diradicals.

**Table 6.5.** Energy of HOMO and LUMO in au and their differences in *eV* and molecular hardness ($\eta$) at the UB3LYP/6-31G(d,p) level for diradicals.

| Diradicals | $E_{HOMO}$ in *au* | $E_{LUMO}$ in *au* | $\Delta E_{HOMO-LUMO}$ in *eV* | Molecular Hardness($\eta$) |
|---|---|---|---|---|
| 1a | –0.19503 | –0.07942 | 3.1459 | 1.5730 |
| 1b | –0.19318 | –0.08107 | 3.0507 | 1.5254 |
| 2a | –0.21286 | –0.09474 | 3.2142 | 1.6071 |
| 2b | –0.21256 | –0.10218 | 3.0036 | 1.5018 |
| 3a | –0.18638 | –0.09803 | 2.4042 | 1.2021 |
| 3b | –0.18323 | –0.09983 | 2.2695 | 1.1347 |

However, Chattaraj and co-workers[46] have advocated over the fact that for open shell spin polarized triplet state the relationship between HOMO–LUMO gap and the stability of the molecules is not as simple as widely assumed. This is because LUMO may come below the HOMO giving a negative contribution to the hardness, as in some cases LUMO is not well defined. It is also known that the molecules having HOMO–LUMO energy gap of the order of 1.59–3.18 *eV* can be used in optoelectronic devices, and in non-linear optical (NLO) imaging.[47] On the other hand, the fluorophores similar to GFP have their uses as optoelectronic devices.[48] In this case all the diradicals have HOMO–LUMO energy gap

2.44–3.14 *eV* (Table 6.5) and can be used for preparing organic light emitting diode (OLED), and in the development of high-density optical memories and switches.[49] The acidic –OH group in GFP makes it less useful as OLED material; nevertheless, efforts are being put to develop oxazolone and imidazolidinone derivatives related to GFP chromophore to overcome this problem.[48]

## 6.4. Conclusions

Magnetic nano- and micro-particles are judiciously used in various biomedical applications.[50] On the other hand, GFP and its different variants also earned substantial attention in the field of molecular biology.[9] The reversible photochromic cis/trans isomerization, which is independent of the nature of the solvents, is displayed by GFP and its different analogous chromophores.[15] In this chapter, six GFP based photoswitchable diradicals are theoretically designed and characterized. These molecules undergo magnetization reversal associated with change in color, which are likely to receive attention in the field of biomedical applications. A general schematic representation (Scheme 6.3) shows such magnetic reversal in all our designed GFP based diradicals from bright fluorescent cis form to their dark trans form. The extent of magnetic interactions in all six molecules have been quantified in terms of the coupling constant through unrestricted broken symmetry approach in the framework of density functional theory. In our investigated systems, antiferromagnetic dark trans isomers turn into bright fluorescing ferromagnetic cis forms when exposed to light in the wavelength range 360-390 nm. Thus, one can observe cyan, blue and green colours for systems 1, 2 and 3 respectively, when magnetic crossover takes place. From DOS plots it is clear that at Fermi level the spins are highly polarized for ferromagnetic cis diradicals, which indicates such molecules will show a spin valve effect. We have also compared the ground state stabilities of these diradicals and find that the ferromagnetic cis isomer is more stable than respective antiferromagnetic one. The HOMO–LUMO energy gap indicates that the diradicals can be used in NLO imaging. It can also be used to prepare OLED devices, high-density optical memories and switches.[48,49]

**Scheme 6.3.** A general schematic representation of magnetic reversal of GFP based diradicals from bright fluorescent cis form to their dark trans form.

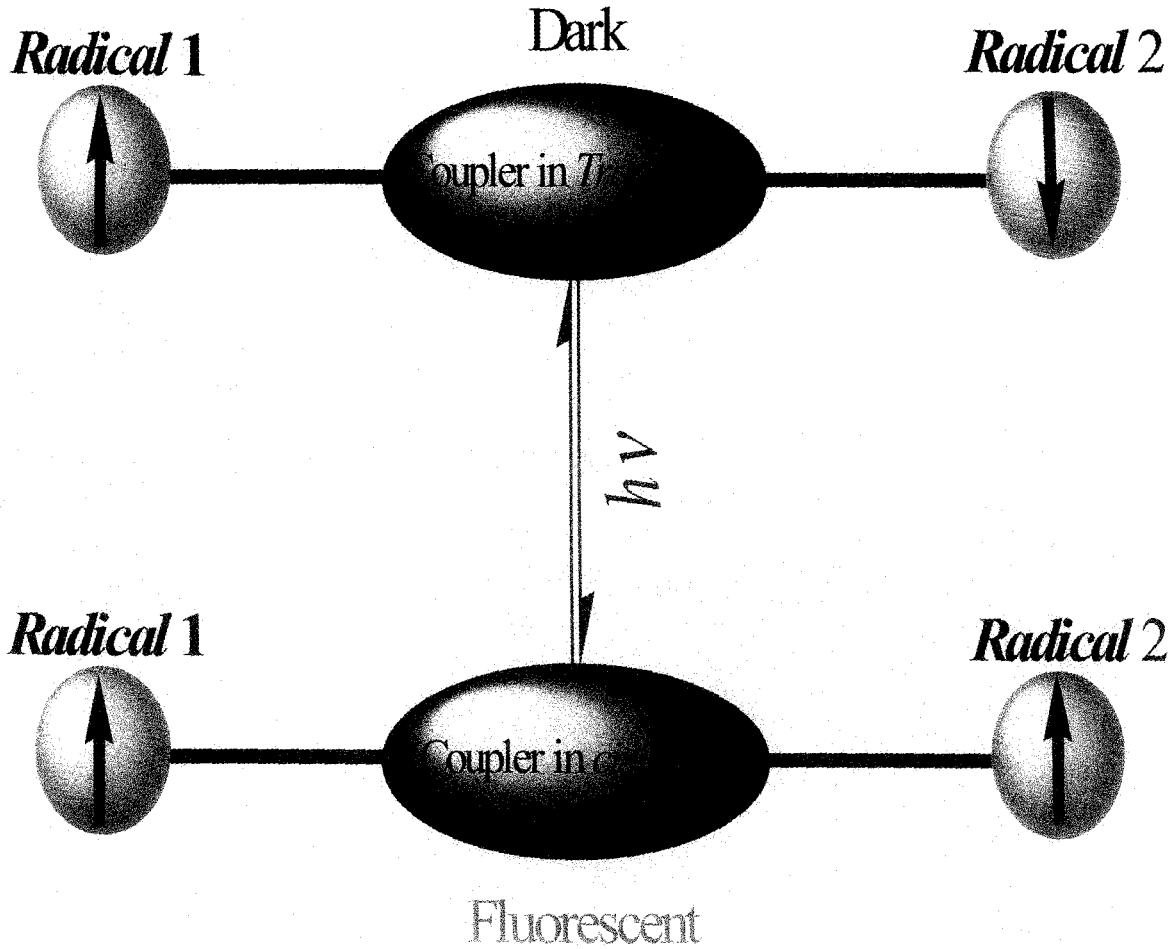


Recently, in an interesting work, Weber et al. have addressed the use of magnet guided transduction of enhanced GFP encoded lentiviral particles coupled with three layers carbon coated cobalt based nanoparticle in targeted delivery of therapeutic transgene to the pathologic tissue.[51] The capacity of magnetic folate conjugate nanoparticle towards its tagging ability in the cancerous cell with the reduction of unwanted side effects and toxicity has been shown by Pramanik and co-workers.[52] However, GFP functions as magnetic drug carrier without any biocompatible coating; moreover, GFP based multifunctional magnetic drug carrier can also act as a biological magnetic tagger which can be traced with the change in color associated with magnetization reversal. In the first step, GFP based magnetic drug

carriers can label the living cells *in vivo* and then magnetic separation of desired biological entity is possible. GFP based diradicals attached with multifunctional drugs can congregate at the required pathological site by local or external control. In the next step, it can discharge the specific drug at precise target or one can treat it by hyperthermia. GFP based fluorescent magnetic particles can be utilized as a multidimensional tool to molecular biologists; i.e., it can assist to test drug effectiveness or can help to act as a drug carrier in controlled drug delivery *in vivo*. Contrast agents, such as nitroxyls or aminoxyls, are used in magnetic resonance imaging (MRI) to enhance the image quality.[53] Here we have imino nitroxide moieties in the diradicals; hence, such multifunctional diradicals might also be used as a contrast agent in MRI. Last but not the least; it is needless to say photocontrol of magnetic crossover in GFP based diradicals make them suitable for next generation biomedical research.

**This work has been published in Photochemistry photobiology A: Chemistry (Ref. 54).**

## 6.5. References and Notes


(1) Shimomura, O.; Johnson, F. H.; Saiga, Y. *J. Cell. Comp. Physiol.* **1962**, *59*, 223.

(2) Tsien, R. Y. *Annu. Rev. Biochem.* **1998**, *67*, 509.

(3) Prasher, D. C.; Eckenrode, V. K.; Ward, W. W.; Pendergast, F. G.; Cormier, M. J. *Gene* **1992**, *111*, 229.

(4) Zimmer, M. *Chem. Rev.* **2002**, *102*, 759.

(5) Chan, A. W. S.; Chong, K. Y.; Martinovich, C.; Simerly, C.; Schatten, G. *Science* **2001**, *29*, 309.

(6) Bogdanov, A. M.; Mishin, A. S.; Yampolsky, I. V.; Belousov, V. V.; Chudakov, D. M.; Subach, F. V.; Verkhusha, V. V.; Lukyanov, S.; Lukyanov, K. A. *Nat. Chem. Biol.* **2009**, *5*, 459.

(7) Gory, L.; Montel, M. C.; Zagorec, M. *FEMS Microbiol. Lett.* **2001**, *194*, 127.

(8) See link: http://www.nasa.gov/mission_pages/station/science/experiments/TAGES.html

(9) Dickson, R. M.; Cubitt, A. B.; Tsien, R. Y.; Moerner, W. E. *Nature* **1997**, *388*, 355.

(10) Dong, J.; Solntsev, K. M.; Poizat, O.; Tolbert, L. M. *J. Am. Chem. Soc.* **2007**, *129*, 10084.

(11) Chen, K. Y.; Cheng, Y. M.; Lai, C. H.; Hsu, C. C.; Ho, M. L.; Lee, G. H.; Chou, P. T. *J. Am. Chem. Soc.* **2007**, *129*, 4534.

(12) Matsuda, K.; Irie, M. *J. Am. Chem. Soc.* **2000**, *122*, 7195.

(13) Ali, Md. E.; Datta, S. N. *J. Phys. Chem. A* **2006**, *110*, 10525.

(14) Shil, S.; Misra, A. *J. Phys. Chem. A* **2010**, *114*, 2022.

(15) Voliani, V.; Bizzarri, R.; Nifosí, R.; Abbruzzetti, S.; Grandi, E.; Viappiani, C.; Beltram, F. *J. Phys. Chem. B* **2008**, *112*, 10714.

(16) Grigorenko, B.; Savitsky, A.; Topol, I.; Burt, S.; Nemukhin, A. *Chem. Phys. Lett.* **2006**, *424*, 184.

(17) Ullman, E. F.; Boocock, D. G. B. *J. Chem. Soc. D: Chem. Commun.* **1969**, 1161.

(18) Koivisto, B. D.; Hicks, R. G. *Coord. Chem. Rev.* **2005**, *249*, 2612.

(19) Noodleman, L. *J. Chem. Phys.* **1981**, *74*, 5737.

(20) Ginsberg, A. P. *J. Am. Chem. Soc.* **1980**, *102*, 111.

(21) Noodleman, L.; Peng, C. Y.; Case, D. A.; Mouesca, J. M. *Coord. Chem. Rev.* **1995**, *144*, 199.

(22) Noodleman, L.; Davidson, E. R. *Chem. Phys.* **1986**, *109*, 131.

(23) Bencini, A.; Totti, F.; Daul, C. A.; Doclo, K.; Fantucci, P.; Barone, V. *Inorg. Chem.* **1997**, *36*, 5022.

(24) Ruiz, E.; Cano, J.; Alvarez, S.; Alemany, P. *J. Comput. Chem.* **1999**, *20*, 1391.

(25) Yamaguchi, K.; Takahara, Y.; Fueno, T.; Nasu, K. *Jpn. J. Appl. Phys.* **1987**, *26*, L1362.

(26) (a) Polo, V.; Alberola, A.; Andres, J.; Anthony, J.; Pilkington, M. *Phys. Chem. Chem. Phys.* **2008**, *10*, 857. (b) Bhattacharya, D.; Misra, A. *J. Phys. Chem.* A **2009**, *113*, 5470. (c) Bhattacharya, D.; Shil, S.; Misra, A.; Klein, D. J. *Theor. Chem. Acc.* **2009**, *127*, 57.

(27) Neese, F. *J. Phys. Chem. Solids* **2004**, *65*, 781.

(28) Kitagawa, Y.; Saito, T.; Nakanishi, Y.; Kataoka, Y.; Matsui, T.; Kawakami, T.; Okumura, M.; Yamaguchi, K. *J. Phys. Chem. A* **2009**, *113*, 15041.

(29) Scalmani, G.; Frisch, M. J.; Mennucci, B.; Tomasi, J.; Cammi, R.; Barrone, V. *J. Chem. Phys.* **2006**, *124*, 094107.

(30) Seth, M.; Ziegler, T. *J. Chem. Phys.* **2005**, *123*, 144105.

(31) Casida, M. E.; Jamorski, C.; Casida, K. C.; Salahub, D. R. *J. Chem. Phys.* **1998**, *108*, 4439.

(32) Bauernschmitt, R.; Ahlrichs, R. *Chem. Phys. Lett.* **1996**, *256*, 454.

(33) Bauernschmitt, R.; Ahlrichs, R. *J. Chem. Phys.* **1996**, *104*, 9047.

(34) Čížek, J.; Paldus, J. *J. Chem. Phys.* **1967**, *47*, 3976.

(35) Frisch, M. J.; Trucks, G. W.; Schlegel, H. B.; Scuseria, G. E.; Robb, M. A.; Cheeseman, J. R.; Montgomery, J. A. Jr.; Vreven, T.; Kudin, K. N.; Burant, J. C.; Millam, J. M.; Iyengar, S. S.; Tomasi, J. J.; Barone, V.; Mennucci, B.; Cossi, M.; Scalmani, G.; Rega, N.; Petersson, G. A.; Nakatsuji, H.; Hada, M.; Ehara, M.; Toyota, K.; Fukuda, R.; Hasegawa, J ; Ishida, M.; Nakajima, T.; Honda, Y.; Kitao, O.; Nakai, H.; Klene, M.; Li, X.; Knox, J. E.; Hratchian, H. P.; Cross, J. B.; Bakken, V.; Adamo, C.; Jaramillo, J.; Gomperts, R.; Stratmann, R. E.; Yazyev, O.; Austin, A. J.; Cammi, R.; Pomelli, C.; Ochterski, J.; Ayala, P. Y.; Morokuma, K.; Voth, A.; Salvador, P.; Dannenberg, J. J.; Zakrzewski, V. G.; Dapprich, S.; Daniels, A. D.; Strain, M. C.; Farkas, O.; Malick, D. K.; Rabuck, A. D.; Raghavachari, K.; Foresman, J. B.; Ortiz, J. V.; Cui, Q.; Baboul, A. G.; Clifford. S.; Cioslowski, J.; Stefanov, B. B.; Liu, G.;

Liashenko, A.; Piskorz, P.; Komaromi, I.; Martin, R. L.; Fox, D. J.; Keith, T.; Al-Laham, M. A.; Peng, C. Y.; Nanayakkara, A.; Challacombe, M.; Gill, P. M. W.; Johnson, B.; Chen, W.; Wong, M. W.; Gonzalez, C.; Pople, J. A. GAUSSIAN 03W (Revision D.01), Gaussian, Inc.: Wallingford, CT, (2004).

(36) Trindle, C.; Datta, S. N. *Int. J. Quantum Chem.* **1996**, *57*, 781.

(37) Thirion, C.; Wernsdorfer, W.; Mailly, D. *Nat. Mater.* **2003**, *2*, 524.

(38) Rinkevicius, Z.; Tunell, I.; Salek, P.; Vahtras, O.; Agren, H. *J. Chem. Phys.* **2003**, *119*, 34.

(39) Radziszewski, J. G.; Gil, M.; Gorski, A.; Larsen, J. S.; Waluk, J.; Mroz, B. J. *J. Chem. Phys.* **2001**, *115*, 9733.

(40) Hirata, S.; Lee, T. J.; Gordon, M. H. *J. Chem. Phys.* **1999**, *111*, 8904.

(41) Liu, R.; Ke, S. H.; Baranger, H. U.; Yang, W. *Nano Lett.* **2005**, *5*, 1959.

(42) O'Boyle, N. M.; Tenderholt, A. L.; Langner, K. M. *J. Comput. Chem.* **2008**, *29*, 839.

(43) Westcott, B. L.; Gruhn, N. E.; Michelsen, L. J.; Lichtenberger, D. L. *J. Am. Chem. Soc.* **2000**, *122*, 8083.

(44) Franceschetti, A.; Zunger, A. *Europhys. Lett.* **2000**, *50*, 243.

(45) Latif, I. A.; Panda, A.; Datta, S. N. *J. Phys. Chem. A* **2009**, *113*, 1595.

(46) Fuentealba, P.; Simon-Manso, Y.; Chattaraj, P. K. *J. Phys. Chem. A* **2000**, *104*, 3185.

(47) Khatchatouriants, A.; Lewis, A.; Rothman, Z.; Loew, L.; Treinin, M. *Biophy. J.* **2000**, *79*, 2345.

(48) You, Y.; Yingke, H.; Burrows, P. E.; Forrest, S. R.; Petasis, N. A.; Thompson, M. E. *Adv. Mater.* **2000**, *12*, 1678.

(49) Cinelli, R. A. G.; Pellegrini, V.; Ferrari, A.; Faraci, P.; Nifosí, R.; Tyagi, M.; Giacca, M.; Beltram, F. *Appl. Phys. Lett.* **2001**, *79*, 3353.

(50) Pankhurst, Q. A.; Connolly, J.; Jones, S. K.; Dobson, J. *J. Phys. D: Appl. Phys.* **2003**, *36*, R167.

(51) Weber, W.; Lienhart, C.; Baba, M. D.; Grass, R. N.; Kohler, T.; Müller, R.; Stark, W. J.; Fussenegger, M. *J. Biotechnol.* **2009**, *141*, 118.

(52) Mohapatra, S.; Mallick, S. K.; Maiti, T. K.; Ghosh, S. K.; Pramanik, P. *Nanotechnology* **2007**, *18*, 385102.

(53) Sosnovsky, G.; Rao, N. U. M.; Li, S. W.; Swartz, H. M. *J. Org. Chem.* **1989**, *54*, 3667.

(54) Bhattacharya, D.; Shil, S.; Misra, A. *J. Photochem. Photobiol. A: Chem.* **2011**, *217*, 402.